Antimicrobial Activity

Deutsche Ausgabe: DOI: 10.1002/ange.201602965
Internationale Ausgabe: DOI: 10.1002/anie.201602965

Engineering Gram Selectivity of Mixed-Charge Gold Nanoparticles by Tuning the Balance of Surface Charges

*Pramod P. Pillai[+], Bartlomiej Kowalczyk[+], Kristiana Kandere-Grzybowska, Magdalena Borkowska, and Bartosz A. Grzybowski**

Abstract: *Nanoparticles covered with ligand shells comprising both positively and negatively charged ligands exhibit Gram-selective antibacterial action controlled by a single experimental parameter, namely the proportion of [+] and [−] ligands tethered onto these particles. Gram selectivity is attributed to the interplay between polyvalent electrostatic and non-covalent interactions that work in unison to disrupt the bacterial cell wall. The [+/−] nanoparticles are effective in low doses, are non-toxic to mammalian cells, and are tolerated well in mice. These results constitute the first example of rational engineering of Gram selectivity at the (macro)molecular level.*

While new classes of antibiotics are being discovered[1] and the existing ones are being optimized in increasingly rational ways,[2] there are still no systematic means to predict and/or adjust the selectivity of antimicrobial agents against Gram-positive versus Gram-negative bacteria. These two classes of bacteria differ not only in the structure and molecular composition of the cell wall but also in terms of the net surface charge.[3] Herein, we capitalize on this charge difference and demonstrate that Gram selectivity can be controlled by a single experimental parameter, namely the proportion of positively and negatively charged ligands tethered onto nanoscopic particles. Remarkably, while purely negative nanoparticles do not interact with the negatively charged bacteria at all and the (widely studied[4]) fully positive nanoparticles exhibit only modest antibacterial activity, certain intermediate ratios of [+/−] ligands tethered onto mixed-charge nanoparticles result in potent and Gram-selective antibacterial action. We attribute this effect to the balance between polyvalent[5] electrostatic and non-covalent interactions that work in unison to disrupt the bacterial cell wall. The [+/−] NPs are effective in low doses (50–200 nM vs. 100 nM −1 μM for conventional antibiotics[6a]), are non-toxic to mammalian cells, and are tolerated well in mice, suggesting future opportunities in developing these mixed-charge constructs for medical applications.

The observation that bacterial cell wall is negatively charged is not new and has been used to design several types of cationic antimicrobials including peptides,[6] polymers,[2f,7] and nanoparticles,[4,8] the latter achieving high potency against multiple-drug-resistant strains but no Gram selectivity.[9] On the other hand, much less attention has been paid to the fact that Gram-negative bacteria have higher negative surface charge that Gram-positive ones.[3] We reasoned that this difference could provide a basis for the design of Gram-selective antimicrobials. Accordingly, we focused on nanoparticles covered with mixed self-assembled monolayers, mSAMs,[10] of cationic ligands (mediating electrostatic interactions) and acidic ligands (potentially competing for the hydrogen bonds within the bacterial cell wall). The choice of such mixed-charge NPs was further motivated by the ability to control ligand shell composition (and thus the magnitude of electrostatic interactions) to within few percent.[11]

We used gold nanoparticles, AuNPs, having core diameters $d = 2.5 \pm 0.6$ nm, 5.2 ± 0.5 nm, or 9.5 ± 0.8 nm and functionalized with mSAMs comprising *N,N,N*-trimethyl(11-mercaptoundecyl) ammonium chloride, TMA, and either (i) 11-mercapto-1-undecylsulfonic acid, MUS, (ii) 11-mercapto-1-undecylphosphonic acid, MUP, or (iii) 11-mercaptoundecanoic acid, MUA. For the TMA/MUS pair, the ligand exchange reaction was problematic as the dodecylamine-covered DDA NP precursors, the TMA, and the MUS thiols could not all be readily solubilized in the same solvent/solvent mixture. For the TMA/MUP particles, the pH had to be very high to fully deprotonate these groups, or the charge of the NPs changed strongly, and was thus hard to control, upon even small changes in pH between the $pK_{a,1}$ and $pK_{a,2}$ of the acid. The TMA/MUA combination proved to be the most experimentally convenient and robust, with TMA ligands positively charged regardless of pH and MUA ligands largely deprotonated and negatively charged at physiological pH ≈ 7.4 (Figure 1 a). Ten types of TMA/MUA AuNPs were prepared that differed in the surface composition as expressed by the relative contents of the oppositely charged ligands on the surfaces of these particles, $\chi_{TMA}:\chi_{MUA}$ (see the Supporting Information for preparation and characterization details). The values of surface compositions were quantified by NMR and, separately, by an electrostatic titration method.[12] These compositions spanned the full range from pure-MUA ($\chi_{TMA}:\chi_{MUA} = 0:100$) to pure-TMA ($\chi_{TMA}:\chi_{MUA} = 100:0$) NPs.

[*] Dr. P. P. Pillai,[+] Dr. B. Kowalczyk[+]
Department of Chemistry and Department of Chemical and Biological Engineering, Northwestern University
2145 Sheridan Road, Evanston, IL 60208 (USA)
Dr. P. P. Pillai[+]
Department of Chemistry
Indian Institute of Science Education and Research (IISER) Pune
Dr. Homi Bhabha Road, Pune, 411008 (India)
Prof. K. Kandere-Grzybowska, Dr. M. Borkowska, Prof. B. A. Grzybowski
IBS Center for Soft and Living Matter and Department of Chemistry
Ulsan National Institute of Science and Technology (UNIST)
Ulsan (South Korea)
E-mail: grzybor72@unist.ac.kr
[+] These authors contributed equally to this work.

Supporting information for this article can be found under: http://dx.doi.org/10.1002/anie.201602965.

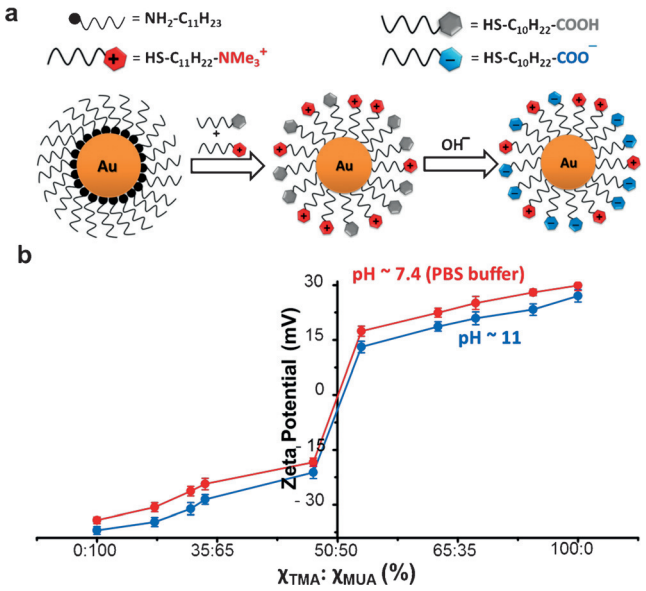

Figure 1. Mixed-charge [+/−] NPs. a) Illustration of the synthesis of mixed-charge TMA/MUA nanoparticles. The relative compositions of these thiols in solution used for NP functionalization and on the resulting NPs are generally different, which is why the latter have to be determined independently by methods such as core etching followed by NMR (Supporting Information). b) Quantification of the NP charge polarities (from zeta potentials[10]) plotted against the composition of the mixed on-particle SAMs (composition expressed as χ_{TMA}:χ_{MUA} ratios as determined by core-etching/NMR analyes). The blue curve is for pH 11 and fully deprotonated MUAs; the red curve is for pH 7.4 (PBS buffer) under which conditions a small fraction of the MUAs is protonated (and hence the curve shifts slightly upwards compared to the one for pH 11). Error bars are based on three separate measurements.

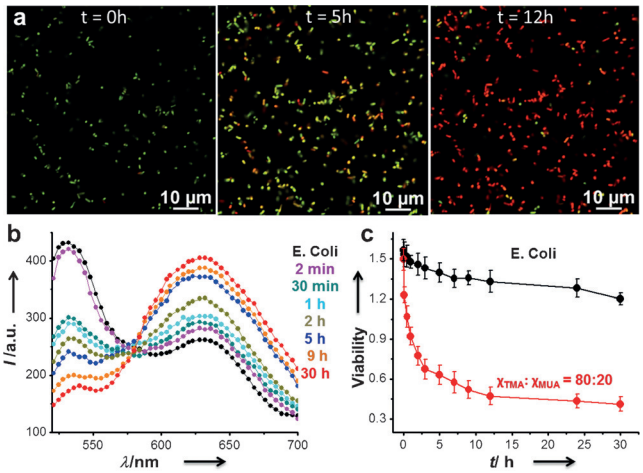

Figure 2. Quantification of antimicrobial activity using a live/dead bacterial viability assay. a) Confocal microscopy images of *E. coli* (2×10^8 per mL) incubated with a mixture of green SYTO 9 and red propidium iodide dyes and a 50 nM suspension of 5.2 nm NPs (χ_{TMA}:χ_{MUA} = 80:20). The three images correspond to different times after incubation. The emergence of red color indicates the bacteria are being killed. b) As part of this bacterial viability assay, fluorescence spectra were recorded at different times (indicated next to the curves). A decrease in the intensity of green emission (I_G at 530 nm) with a simultaneous increase in the intensity of the red emission (I_R at 630 nm) confirms killing of bacteria. c) The concentrations of live bacteria decrease in time as quantified by the I_G/I_R ratio defining viability. The upper black curve is for the suspension of bacteria in PBS but not treated with the [+/−] NPs (see also caption to Figure 3).

The net charge polarities of these particles were quantified by the measurements of their zeta potentials as plotted in Figure 1b for pH 11 and also for pH 7.4 in the PBS buffer.

Antibacterial properties of such NPs against Gram-positive (*Staphylococcus aureus*, *Enterococcus faecium*) and Gram-negative (*Escherichia coli*, *Acinetobacter baumannii*) bacteria were quantified in vitro by a standard cell viability Live/Dead *Bac*Light assay[13] in which a fixed amount of bacteria is first stained with a pair of fluorescent dyes followed by incubation in the presence of the [+/−] NPs at different concentrations. Red and green fluorescence of dyes absorbed by bacteria corresponds directly to the integrity of the bacterial wall and therefore to bacteria's state: dead (red fluorescence) and/or live (green fluorescence) (Figure 2a). The relative intensities of the green and red fluorescence, I_G/I_R, measured using a fluorescence plate reader (Figure 2b) then allow us to quantify (Figure 2c) the antibacterial potency of different types of NPs. Based on this standardized method, we performed a series of experiments in which we screened NPs of different types and sizes over 30 h. The results are summarized in Figure 3 (see also the Supporting Information, Figure S3). As seen, the antibacterial activity depends on the surface composition of the particles (Figure 3a–c). There are four remarkable outcomes of these experiments. First, while both pure-MUA and pure-TMA NPs show only marginal antibacterial activity, this activity is maximized for intermediate surface compositions, $(\chi_{TMA}:\chi_{MUA})_{max}$, with both TMA and MUA ligands present at each NP. Second, the value of $(\chi_{TMA}:\chi_{MUA})_{max}$ is different for Gram-negative and for Gram-positive bacteria. For the former, the most effective nanoparticles have 80% of the TMA ligands on their surfaces while for the latter, the NPs have only 48 surface % of TMA (Figure 3c). What is important, the particles with these surface compositions are specific in the sense that the $(\chi_{TMA}:\chi_{MUA})_{max}$ = 80:20 do not kill Gram-positive bacteria to any appreciable degree, while the $(\chi_{TMA}:\chi_{MUA})_{max}$ = 48:52 NPs do not kill the Gram-negative ones. Third, the rates at which the 80:20 particles kill Gram-negative bacteria are commensurate with the rates of killing of Gram-positive bacteria by the 48:52 NPs (compare similar heights of peaks in Figure 3c); in other words, the selectivity does not compromise the potency (in contrast to some recent studies on purely cationic nanoparticles, whereby killing rates were appreciable only for Gram-positive strains[8b,14]). Fourth, the most effective values $(\chi_{TMA}:\chi_{MUA})_{max}$ are conserved among different Gram-negative and Gram-positive bacteria; that is, they are the same for *E.coli* and *Acinetobacter baumannii* (blue and dark violet lines in Figure 3c) and the same for *Staphylococcus aureus* and *Enterococcus faecium* (dark red and pink lines in Figure 3c). Since the Gram classification is based on the structure of the bacterial cell wall, the last result suggests that our mixed-charge NPs might disrupt this wall with specificity originating from the different surface compositions of the particles. We also note that the killing rate

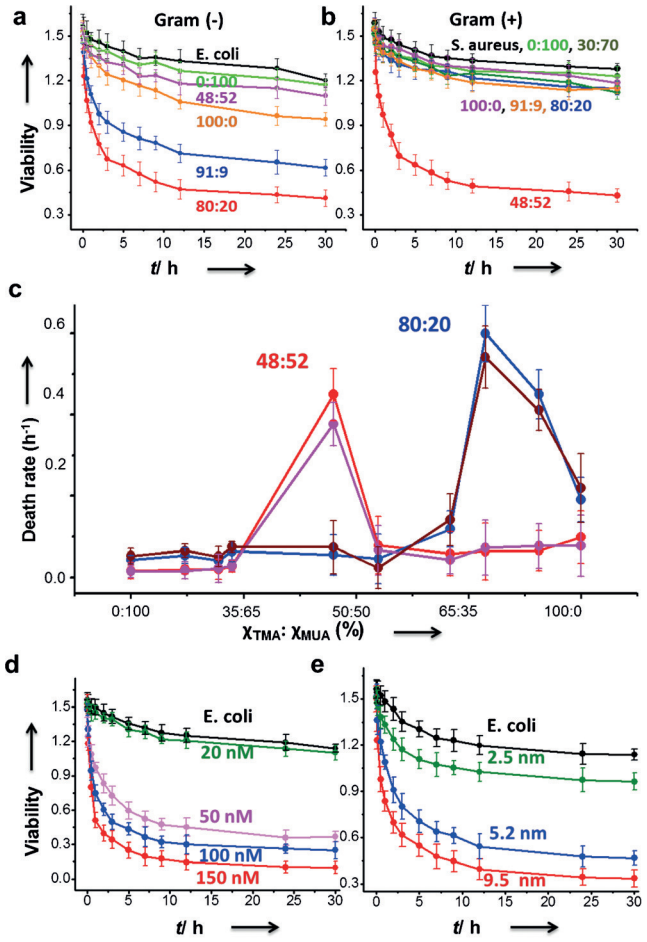

Figure 3. Quantification of antibacterial action and Gram-selectivity of the [+/−] NPs. The viabilities calculated from the ratio of green and red fluorescence quantify the fractions of bacteria surviving with time after incubation with 5.2 nm [+/−] AuNPs. Graph a) is for Gram-negative *Escherichia coli*, 4×10^8 bacteria per mL and b) is for Gram-positive *Staphylococcus aureus*, 2×10^7 bacteria per mL (see the Supporting Information, Figure S3 for similar plots for *Acinetobacter baumannii* and *Enterococcus faecium*). In all experiments, 50 μL of 50 nM AuNPs solution was added to 50 μL of bacteria solution. Numbers next to the curves give the compositions χ_{TMA}:χ_{MUA} of mSAMs decorating the particles. c) Death rates calculated from the dependencies in (a), (b) and in the Supporting Information, Figure S3 and plotted as a function of mSAM composition. Red and pink trends are for Gram-positive *Staphylococcus aureus* and *Enterococcus faecium* bacteria, respectively. Blue and violet trends are for Gram-negative *Escherichia coli* and *Acinetobacter baumannii* bacteria, respectively. Bacteria are killed more effectively by d) more concentrated NP solutions (numbers next to curves give concentrations in nM) and e) by larger particles. Data shown in (d) is for 5.2 nm particles decorated with χ_{TMA}:χ_{MUA} = 80:20 mSAMs. Data shown in (e) is for χ_{TMA}:χ_{MUA} = 80:20 mSAMs for all particle sizes. Black curves in (a,b,d,e) are controls (i.e., bacteria without any NPs). From the procedure according to Invitrogen, the bacteria are in PBS but no nutrients are added since their presence can interfere with the dyes; this is why the black curves go down with time slightly. Error bars in all panels are based on at least three independent experiments for each condition.

increases with NP concentration (Figure 3d) and, perhaps less obviously, with the NP size (though the increase is marginal from 5.2 to 9.5 nm, see Figure 3e). The size dependence is understandable in light of the polyvalent nature of interactions mediated by the NPs; indeed, free MUA or TMA ligands show no antibacterial activity and it is the electrostatic interactions of ligands constrained onto NPs and acting in concert that matters in our system.[15]

To understand better how the [+/−] NPs interact with bacteria, we performed a series of microscopy studies. First, using TEM imaging, we verified that while pure MUA particles do not adsorb onto the surfaces (Figure 4a) of the bacteria, the pure TMA ones cluster/aggregate on the surface of the bacterium (Figure 4b). This can be rationalized by

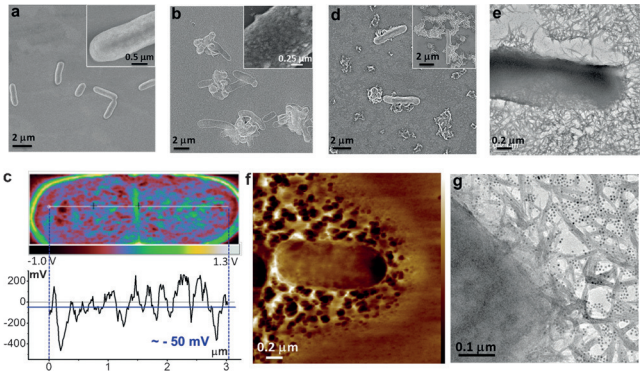

Figure 4. Microscopic studies of bacteria treated with different types of mixed-charge NPs. Scanning electron microscopy (SEM) images of *E. coli* incubated with a) pure-MUA and b) pure-TMA NPs. Inset in (b) shows TMA NPs adsorbing on the bacteria. For TEM images resolving the individual NPs (Supporting Information, Figure S4). c) Kelvin force microscopy (KFM) image of an *E. coli* bacterium illustrating its net negative surface potential of about −50 mV (blue horizontal line). d) SEM, e) TEM, and f) AFM images of *E. coli* after incubation with χ_{TMA}:χ_{MUA} = 80:20 AuNPs evidencing the rupture of the bacterial cell wall. g) TEM image showing χ_{TMA}:χ_{MUA} = 80:20 AuNPs (small dark dots) associated with the intracellular material leaked from the bacterium upon lysis.

Kelvin force microscopy (Figure 4c), which shows that the average electrical potential of the bacterial surface is negative, ca. −50 mV, so it can harbor positively charged NPs. For both MUA and TMA particles, however, the bacterial wall appears intact. This situation changes dramatically for the optimal, $(\chi_{TMA}:\chi_{MUA})_{max}$ compositions of the on-particle monolayers. Such particles cause pronounced rupture of the bacterial wall as evidenced by the intracellular material[16] literally spilling out, as observed both under TEM (Figure 4d,e) and AFM (Figure 4f), and with NPs clearly associated with the disrupted cellular structures (Figure 4g). It is worth noting that the [+/−] NPs retain their mechanism of action against bacteria even after several cycles of antibiotic treatment and re-culturing (Supporting Information, Figure S6); this observation is in line with the results of other studies indicating inability of bacteria to develop effective defense mechanism against physical rupture of the wall.[4a,8a]

Concerning the mechanism of action for the NPs, the following scenario appears plausible. First, our experiments with pure-TMA NPs (compare Figure 4b) confirm that role

of the cationic ligands is to help attach the nanoparticle to the bacterium surface but not necessarily to disrupt the wall (unlike postulated before[4,8]). Since individual TMA ligands (that is, not tethered onto nanoparticles) do not have any adverse effect on the bacteria, polyvalency[5] plays an important role as it eliminates the entropic penalty associated with the adsorption of individual ligands. This penalty can be approximated as $\Delta S \approx kT\ln(A\,d/V)$ for the translational degrees of freedom of each adsorbing species, where $A \approx 3\,\mu m^2$ is the bacterium surface (for example, for roughly spherical *S. aureus*, 1 μm in diameter), $d \approx 1$ nm is the characteristic ligand size, and $V \approx 0.523\,\mu m^3$ is solution volume per one bacterium. It follows that ΔS is only ca. $-2kT$ per ligand but a few hundred kT per 5.5 nm NP with about half of its ligands being TMAs. In reality, this estimate should be corrected for the freezing of some degrees of freedom of NP ligands coming into contact with the bacterium surface; computer simulations[17] indicate, however, that even with such a correction, the free energy of NP-bacterium binding is still highly favorable and on the order of tens of kT. Once polyvalent interactions help attach the particles to the bacterium, the largely deprotonated MUAs can also interact with the cell wall. In particular, the carboxylic acid headgroups can compete for the hydrogen-bonding interactions with lipopolysaccharides and/or peptidoglycans present on the surface of the bacterium and known to contribute to the structural integrity[18] and survival[19] of bacteria. When the hydrogen bonding within the cell wall is disrupted, lysis can ensue.[3,20]

As far as the observed selectivity is concerned, it can be ascribed to Gram-negative bacteria having higher negative surface charge than Gram-positive bacteria.[3] The $(\chi_{TMA}{:}\chi_{MUA})_{max} = 80{:}20$ NPs possessing high positive net charge can interact strongly via electrostatic interactions with the Gram-negative bacteria. In contrast, the $(\chi_{TMA}{:}\chi_{MUA})_{max} = 48{:}52$ NPs have very small and negative net surface charge making them ineffective in binding against highly negatively charged surfaces (that is, Gram-negative bacteria); at the same time, the interactions of such NPs with less-charged Gram-positive bacteria can be facilitated by the presence of more hydrogen-bonding MUA ligands on the surfaces of the particles (cf. preceding paragraph). Also, in the Gram-positive bacteria, the specific feature of the cell wall is the presence of the teichoic/lipoteichoic acids which increase wall rigidity by coordinating metal cations; efficient coordination of such cations by deprotonated MUA ligands on the NPs[21] can be another factor adversely affecting integrity of the wall .

None of the NPs that we studied herein showed any adverse effects/cytotoxicity towards normal/healthy mammalian cells. This was described in our previous work[11b] and is further evidenced by the examples in the Supporting Information, Figures S7–S9.

We also performed a series of in vivo studies using NPs with $\chi_{TMA}{:}\chi_{MUA} = 80{:}20$ as an example and evaluating the in vivo toxicity level in mice (Table 1; Supporting Information, Figure S10). The particles did not cause any adverse effects up to 2 nmol kg^{-1} (200 nM of AuNPs), which was the maximum tolerated dose (MTD) administered via intravenous injection and well above the 50 nM concentrations shown effective in in vitro experiments (compare Figure 2, Figure 3). At 2.5 nmol kg^{-1}, the mice began to tremble with labored breathing. For higher doses, the mice died after AuNP injection. Analyses by inductively coupled plasma (ICP) and pharmacokinetic studies (Supporting Information, Figure S11) also indicated that the NPs localized preferentially to the liver (28%) and lungs (17%), which may explain the breathing difficulties at doses above MTD.

Table 1: Response of mice (4 per condition) to 80:20 AuNPs.[a]

	NP Dosage [nmol/kg mouse]			
	0.5, 1.0, 1.5, 2.0	2.5	3.0	4.0, 10.0
Maximum Tolerated Dose (MTD)	All mice appeared normal after NP injection	All mice began trembling for 1–2 min but then returned to normal	All mice began trembling; 2 mice died, two returned to normal	All mice died immediately

[a] See the Supporting Information for details.

In summary, selective activity of mixed-charge nanoparticles against Gram-positive and Gram-negative bacteria depends solely on the ratio of [+] to [−] ligands on their surfaces. These NPs are straightforward to synthesize in large quantities, are non-toxic towards mammalian cells, do not elicit bacterial resistance, and their effective in vitro dose is tolerated well in mice, all suggesting that surface-charge engineering can be a promising route to nanoparticle-based antibiotics. At the same time, more work (and perhaps large-scale computer simulations) is needed to understand in molecular detail how the [+/−] NPs interact with the cell wall in Gram-specific fashion.

Acknowledgements

The authors thank Dr. T. M. Hermans for confocal imaging and Dr. H. T. Baytekin for AFM/KFM imaging. This work was supported by the Non-Equilibrium Energy Research Center (NERC), which is an EFRC center funded by the U.S. Department of Energy under award DE-SC0000989, the NIH Awards no. 1R21CA137707-01 and no. U54CA119341, and the Institute for Basic Science Korea, Project Code IBS-R020-D1, all to B.A.G.

Keywords: antibiotics · Gram specificity · ligands · nanoparticles · surface charge

How to cite: *Angew. Chem. Int. Ed.* **2016**, *55*, 8610–8614
Angew. Chem. **2016**, *128*, 8752–8756

[1] a) L. L. Ling, T. Schneider, A. J. Peoples, A. L. Spoering, I. Engels, B. P. Conlon, A. Mueller, T. F. Schäberle, D. E. Hughes, S. Epstein, M. Jones, L. Lazarides, V. A. Steadman, D. R. Cohen, C. R. Felix, K. A. Fetterman, W. P. Millett, A. G. Nitti, A. M.

Zullo, C. Chen, K. Lewis, *Nature* **2015**, *517*, 455 – 459; b) L. Kim, *Nat. Rev. Drug. Dis.* **2013**, *12*, 371 – 387; c) L. L. Silver, *Nat. Biotechnol.* **2014**, *32*, 1102 – 1104; d) C. Walsh, *Nat. Rev. Microbiol.* **2003**, *1*, 65 – 70.

[2] a) B. T. Wimberly, *Curr. Opin. Invest. Drugs* **2009**, *10*, 750 – 765; b) J. B. Veselinović, A. A. Toropov, A. P. Toropova, G. M. Nikolić, A. M. Veselinović, *Arch. Pharm.* **2015**, *348*, 62 – 67; c) A. Speck-Planche, M. N. D. S. Cordeiro, *ACS Comb. Sci.* **2014**, *16*, 78 – 84; d) P. Rondon-Villarreal, D. A. Sierra, R. Torres, *Curr. Comput.-Aided Drug Des.* **2014**, *10*, 183 – 190; e) C. Loose, K. Jensen, I. Rigoutsos, G. Stephanopoulos, *Nature* **2006**, *443*, 867 – 869; f) G. N. Tew, R. W. Scott, M. L. Klein, W. F. DeGrado, *Acc. Chem. Res.* **2010**, *43*, 30 – 39.

[3] Y. Shai, *Biopolymers* **2002**, *66*, 236 – 248.

[4] a) L. Liu, K. Xu, H. Wang, P. K. J. Tan, W. Fan, S. S. Venkatraman, L. Li, Y. Yang, *Nat. Nanotechnol.* **2009**, *4*, 457 – 463; b) S. C. Hayden, G. Zhao, K. Saha, R. L. Phillips, X. Li, O. R. Miranda, V. M. Rotello, M. A. El-Sayed, I. Schmidt-Krey, U. H. F. Bunz, *J. Am. Chem. Soc.* **2012**, *134*, 6920 – 6923; c) Y. Zhao, X. Jiang, *Nanoscale* **2013**, *5*, 8340 – 8350.

[5] M. Mammen, S.-K. Choi, G. M. Whitesides, *Angew. Chem. Int. Ed.* **1998**, *37*, 2754 – 2794; *Angew. Chem.* **1998**, *110*, 2908 – 2953.

[6] a) Y. J. Gordon, E. G. Romanowski, *Curr. Eye Res.* **2005**, *30*, 505 – 515; b) H. G. Boman, *Cell* **1991**, *65*, 205 – 207; c) R. E. W. Hancock, H. G. Sahl, *Nat. Biotechnol.* **2006**, *24*, 1551 – 1557; d) K. A. Brogden, *Nat. Rev. Microbiol.* **2005**, *3*, 238 – 250.

[7] a) V. Sambhy, B. R. Peterson, A. Sen, *Angew. Chem. Int. Ed.* **2008**, *47*, 1250 – 1254; *Angew. Chem.* **2008**, *120*, 1270 – 1274; b) A. M. Carmona-Ribeiro, L. D. de Melo Carrasco, *Int. J. Mol. Sci.* **2013**, *14*, 9906 – 9946; c) S. R. Deka, A. K. Sharma, P. Kumar, *Curr. Top. Med. Chem.* **2015**, *15*, 1179 – 1195.

[8] a) F. Nederberg, Y. Zhang, J. P. K. Tan, K. Xu, H. Wang, C. Yang, S. Gao, X. D. Guo, K. Fukushima, L. Li, J. L. Hedrick, Y.-Y. Yang, *Nat. Chem.* **2011**, *3*, 409 – 414; b) Z. V. Feng, I. L. Gunsolus, T. A. Qiu, K. R. Hurley, L. H. Nyberg, H. Frew, K. P. Johnson, A. M. Vartanian, L. M. Jacob, S. E. Lohse, M. D. Torelli, R. J. Hamers, C. J. Murphy, C. L. Haynes, *Chem. Sci.* **2015**, *6*, 5186 – 5196.

[9] X. Li, S. M. Robinson, A. Gupta, K. Saha, Z. Jiang, D. F. Moyano, A. Sahar, M. A. Riley, V. M. Rotello, *ACS Nano* **2014**, *8*, 10682 – 10686.

[10] S. C. Love, L. A. Estroff, J. K. Kriebel, R. G. Nuzzo, G. M. Whitesides, *Chem. Rev.* **2005**, *105*, 1103 – 1169.

[11] a) A. M. Kalsin, B. Kowalczyk, P. Wesson, B. A. Grzybowski, *J. Am. Chem. Soc.* **2007**, *129*, 6664 – 6665; b) P. P. Pillai, S. Huda, B. Kowalczyk, B. A. Grzybowski, *J. Am. Chem. Soc.* **2013**, *135*, 6392 – 6395.

[12] P. P. Pillai, B. Kowalczyk, W. J. Pudlo, B. A. Grzybowski, *J. Phys. Chem. C* **2016**, *120*, 4139 – 4144.

[13] a) P. Li, Y. F. Poon, W. Li, H.-Y. Zhu, S. H. Yeap, Y. Cao, X. Qi, C. Zhou, M. Lamrani, R. W. Beuerman, E.-T. Kang, Y. Mu, C. M. Li, M. W. Chang, S. S. J. Leong, M. B. Chan-Park, *Nat. Mater.* **2011**, *10*, 149 – 156; b) S. Zhao, Y. Li, H. Yin, Z. Liu, E. Luan F. Zhao, Z. Tang, S. Liu, *Sci. Adv.* **2015**, *1*, e1500372.

[14] L. Liu, J. Yang, J. Xie, Z. Luo, J. Jiang, Y. Y. Yang, S. Liu, *Nanoscale* **2013**, *5*, 3834 – 3840.

[15] For a discussion of polyvalent interactions between charged NPs and surfaces, see: B. Kowalczyk, K. J. Bishop, I. Lagzi, D. Wang, Y. Wei, S. Han, B. A. Grzybowski, *Nat. Mater.* **2012**, *11*, 227 – 232.

[16] A. Taglietti, Y. A. Diaz Fernandez, E. Amato, L. Cucca, G. Dacarro, P. Grisoli, V. Necchi, P. Pallavicini, L. Pasotti, M. Patrini, *Langmuir* **2012**, *28*, 8140 – 8148.

[17] a) S. Wang, E. E. Dormidontova, *Soft Matter* **2011**, *7*, 4435 – 4445; b) S. Wang, E. E. Dormidontova, *Phys. Rev. Lett.* **2012**, *109*, 238102.

[18] a) C. Raetz, C. Whitfield, *Annu. Rev. Biochem.* **2002**, *71*, 635 – 700; b) J. van Heijenoort, *Glycobiology* **2001**, *11*, 25R – 36R.

[19] R. S. Munford, *Infect. Immun.* **2008**, *76*, 454 – 465.

[20] S. Cho, Q. Wang, C. P. Swaminathan, D. Hesek, M. Lee, G. J. Boons, S. Mobashery, R. A. Mariuzza, *Proc. Natl. Acad. Sci. USA* **2007**, *104*, 8761 – 8766.

[21] D. Wang, B. Tejerina, I. lagzi, B. Kowalczyk, B. A. Grzybowski, *ACS Nano* **2011**, *5*, 530 – 536.

Received: March 25, 2016
Published online: June 2, 2016

